# Photonic spin Hall effect in topological insulators

Xinxing Zhou, Jin Zhang, Xiaohui Ling, Shizhen Chen, Hailu Luo,* and Shuangchun Wen†

*Key Laboratory for Micro-/Nano-Optoelectronic Devices of Ministry of Education, College of Physics and Microelectronic Science, Hunan University, Changsha 410082, People's Republic of China*

(Received 21 July 2013; published 25 November 2013)

In this paper we theoretically investigate the photonic spin Hall effect (SHE) of a Gaussian beam reflected from the interface between air and topological insulators (TIs). The photonic SHE is attributed to spin-orbit coupling and manifests itself as in-plane and transverse spin-dependent splitting. We reveal that the spin-orbit coupling effect in TIs can be routed by adjusting the axion angle variations. We find that, unlike the transverse spin-dependent splitting, the in-plane one is sensitive to the axion angle. It is shown that the polarization structure in the magneto-optical Kerr effect is significantly altered due to the spin-dependent splitting in the photonic SHE. We theoretically propose a weak measurement method to determine the strength of axion coupling by probing the in-plane splitting of the photonic SHE.

DOI: 10.1103/PhysRevA.88.053840 PACS number(s): 42.25.−p, 42.79.−e, 41.20.Jb

## I. INTRODUCTION

The spin Hall effect (SHE) is a transport effect of inducing transverse spin currents perpendicular to the applied electric-field direction [1,2]. The SHE offers a promising method for spatially separating electron spins which could be applied to develop new spintronic devices [3]. It is well known that the physical mechanism of the SHE in electric systems is attributed to the spin-orbit coupling. Recently, a material known as a topological insulator (TI) has aroused tremendous interest [4,5]. It has gapless helical surface states owing to the topological protection of the time-reversal symmetry and represents a full energy gap in the bulk [6–8]. It is found that an interesting effect named the quantum SHE can exist in TIs due to the spin-orbit coupling. Here the spin-up and spin-down electrons move in opposite directions on the surface edge of TIs with no external magnetic field [9,10]. The quantum SHE holds great potential applications, especially for the development of new spintronic or magnetoelectric devices.

The photonic SHE is a photonic version of the SHE in electronic systems, in which the spin photons play the role of the spin charges and a refractive index gradient plays the role of the applied electric field [11–13]. This effect manifests itself as in-plane and transverse spin-dependent splitting of left- and right-circular components when a spatially confined light beam is reflected or transmitted at an interface. The photonic SHE is currently attracting growing attention and has been intensively investigated in different physical systems such as optical physics [14–17], high-energy physics [18,19], semiconductor physics [20,21], and plasmonics [22–24]. The photonic SHE is generally believed to be a result of an effective spin-orbit coupling that is related to the Berry phase.

In this work, similar to the handling of the electron SHE in TIs with spin-orbit coupling, we evolve the photonic SHE in TIs with spin-orbit coupling that is an interaction of photon spin and the trajectory of beam propagation. The electromagnetic effect called axion coupling can occur in TIs when weak time-reversal breaking perturbation is introduced [7,8]. This coupling is described by the effective Lagrangian density $\mathcal{L}_\Theta = (\alpha\Theta/4\pi^2)\mathbf{E}\cdot\mathbf{B}$. Here, $\alpha = e^2/\hbar c$ is the fine-structure constant and $\Theta$ is the axion angle corresponding to the axion coupling effect. Under this condition, an applied electric field can induce magnetization and a magnetic field can cause polarization. We revealed that, due to the axion coupling effect of TIs, the spin-orbit coupling in the photonic SHE can be modulated by adjusting the axion angle. The field distribution of the reflected beam is analyzed, and we find that the polarization structure in the magneto-optical Kerr effect is significantly altered due to the spin-dependent splitting in the photonic SHE.

The rest of the paper is organized as follows. In Sec. II, we establish a general theoretical model to describe the photonic SHE in TIs. Here the quantitative relationship between the magnitude of the axion angle, spin-dependent shifts, and Kerr rotation angle is established. Next, according to the numerical calculation, we reveal that the in-plane spin-dependent splitting can be modulated by adjusting the axion angle and can occur in the case of horizontal and vertical polarizations showing difference from the usual air-glass interface [25]. However, the transverse spin-dependent splitting is insensitive to the axion coupling variations for a certain range. Additionally, a signal enhancement technique known as weak measurement is theoretically proposed to detect this topological phenomenon. Finally, a conclusion is given in Sec. IV.

## II. THEORETICAL ANALYSIS

Figure 1 schematically illustrates a polarized Gaussian beam reflection at an air-TI interface. When the axion coupling effect appears, the normal rules of electromagnetic wave propagation are modified [7]. As a result, the magneto-optical Kerr effect manifesting for the polarization plane of reflected light acquiring a certain rotation occurs. Importantly, the photonic SHE manifesting for the left- and right-circularly polarized components obtaining opposite shifts can also happen, which is ignored by the previous Kerr effect research. We first theoretically establish the relationship between axion coupling and these two physical phenomena. In this paper, we only consider the incident light beam with horizontal polarization.

*hailuluo@hnu.edu.cn
†scwen@hnu.edu.cn

 

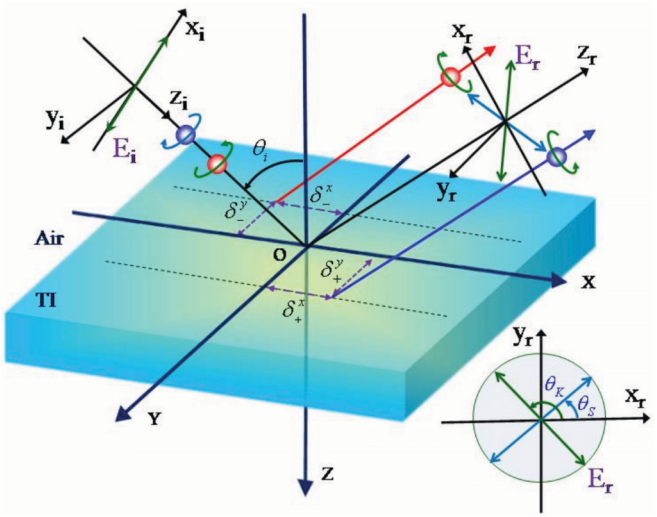


FIG. 1. (Color online) A linearly polarized Gaussian beam reflected on the interface between air and TIs, on which occurs the photonic SHE and magneto-optical Kerr effect. Here, $\theta_i$ is the incident angle. $\delta_{\pm}^{x}$ and $\delta_{\pm}^{y}$ indicate the in-plane (in x direction) and transverse (in y direction) displacements of left- or right-circularly polarized component. The inset: $\theta_K$ stands for the Kerr rotation angle and $\theta_S$ is the spin-dependent splitting rotation angle. We consider the relatively simple external perturbation with magnetic field.

The vertical polarization condition can be analyzed in a similar way. The electromagnetic response of a system under the condition of axion coupling takes the usual Maxwell's equations. We just need to modify the electric displacement $\mathbf{D}$ and magnetic field $\mathbf{H}$ as $\mathbf{D} = \epsilon\mathbf{E} + \alpha(\Theta/\pi)\mathbf{B}$ and $\mathbf{H} = (\mathbf{B}/\mu) - \alpha(\Theta/\pi)\mathbf{E}$ [8]. Here $\alpha = e^2/\hbar c$ is the fine-structure constant and $\Theta$ is the axion angle corresponding to the axion coupling effect, which can be manipulated by the external perturbation with a thin magnetic layer or applying an external static magnetic field perpendicular to the surface. Here we only discuss the relatively simple condition of an external magnetic field.

We first consider the electromagnetic plane-wave reflection on the air-TI interface. One can see that the boundary conditions of the interface with no surface charge or surface current take the usual forms, and so the normal components of $\mathbf{D}$ and $\mathbf{B}$ and the tangential components of $\mathbf{E}$ and $\mathbf{H}$ are also continuous across the interface. With the help of the boundary conditions, we can obtain the $2 \times 2$ Fresnel reflection matrix describing the relations between the incident and the reflection fields (as for the plane wave) [8]:

$$\frac{1}{\Lambda}\begin{bmatrix} (1-n^2-\bar{\alpha}^2)+n\xi_- & 2\bar{\alpha} \\ 2\bar{\alpha} & -(1-n^2-\bar{\alpha}^2)+n\xi_- \end{bmatrix}. \quad (1)$$

Here $\bar{\alpha} = \alpha\Theta/\pi$, $\Lambda = 1+n^2+\bar{\alpha}^2+n\xi_+$, and $\xi_\pm = (\cos\theta_i/\cos\theta_t) \pm (\cos\theta_t/\cos\theta_i)$. The cross-polarized reflection coefficients stem from the term $\bar{\alpha}$ corresponding to the axion coupling, which should be distinguished from the chiral metamaterials [26,27]. In our work, we focus our attention on the photonic SHE and Kerr rotation by considering the incident beam with horizontal polarization. If the axion coupling effect vanishes, the cross-polarized reflection coefficients obtained from the term $\bar{\alpha}$ turn to zero and there is no Kerr rotation, and the reflection matrix can reduce to the normal style [28].

To simplify the following calculation, we can rewrite the reflection matrix from Eq. (1) as

$$\begin{bmatrix} r_{pp} & r_{ps} \\ r_{sp} & r_{ss} \end{bmatrix}. \quad (2)$$

For incident light linearly polarized in the $x$ direction or $y$ direction, the Kerr rotation angle is defined by $\tan\theta_K = E_r^y/E_r^x$. We can see that the Kerr effect manifests itself as the rotation angle of the polarization direction of the reflected light's central wave vector, and so the Kerr rotation angle can be obtained by considering the incident light beam with the Jones vector $(1,0)^T$ or $(0,1)^T$ standing for the horizontal or vertical polarization. The results can be written as $\tan\theta_K = r_{sp}/r_{pp}$ or $\tan\theta_K = r_{ss}/r_{ps}$ for horizontal or vertical polarization incident light. We note that there is no Kerr rotation when the cross-polarized reflection coefficients $r_{sp}$ and $r_{ps}$ are equal to zero, and so the Kerr rotation discussed here originates from the axion coupling effect.

Next we study the photonic SHE and calculate the corresponding displacements of in-plane and transverse spin-dependent splitting, respectively. Let us first consider the paraxial beam reflection on the TIs interface. In the spin basis set, the angular spectrum can be written as $\tilde{\mathbf{E}}_i^H = (\tilde{\mathbf{E}}_{i+} + \tilde{\mathbf{E}}_{i-})/\sqrt{2}$ and $\tilde{\mathbf{E}}_i^V = i(\tilde{\mathbf{E}}_{i-} - \tilde{\mathbf{E}}_{i+})/\sqrt{2}$. The positive and negative signs in the subscripts denote the left- and right-circularly polarized (spin) components. In paraxial optics, the incident field of a localized wave packet whose spectrum is arbitrarily narrow can be written as

$$\widetilde{\mathbf{E}}_{i\pm} = (\mathbf{e}_{ix} + i\sigma\mathbf{e}_{iy})\frac{w_0}{\sqrt{2\pi}}\exp\left[-\frac{w_0^2\left(k_{ix}^2+k_{iy}^2\right)}{4}\right], \quad (3)$$

where $w_0$ is the beam waist. The polarization operator $\sigma = \pm 1$ corresponds to left- and right-circularly polarized light.

To accurately describe the in-plane and transverse spin-dependent splitting, we need to determine the reflection of arbitrary wave-vector components. After the coordinate rotation, and combining with Eq. (2), we can obtain the reflected angular spectrum by means of the relation $\tilde{\mathbf{E}}_r(k_{rx},k_{ry}) = \mathbf{M}_R\tilde{\mathbf{E}}_i(k_{ix},k_{iy})$ [29]. Here $\mathbf{M}_R$ stands for

$$\begin{bmatrix} r_{pp} + \frac{k_{ry}\cot\theta_i(r_{sp}-r_{ps})}{k_0} & r_{ps} + \frac{k_{ry}\cot\theta_i(r_{pp}-r_{ss})}{k_0} \\ r_{sp} - \frac{k_{ry}\cot\theta_i(r_{pp}-r_{ss})}{k_0} & r_{ss} + \frac{k_{ry}\cot\theta_i(r_{sp}-r_{ps})}{k_0} \end{bmatrix}. \quad (4)$$

In the above equations, $r_{pp}$, $r_{ps}$, $r_{sp}$, and $r_{ss}$ denote Fresnel reflection coefficients according to Eq. (2). $k_0$ is the wave number in free space. By making use of a Taylor series expansion based on the arbitrary angular spectrum component, we expand the Fresnel reflection coefficients around the central wave vector for considering the tiny in-plane spread of wave vectors:

$$r_{ab} = r_{ab}(\theta_i) + \frac{\partial r_{ab}}{\partial\theta_i}\frac{k_{ix}}{k_0}. \quad (5)$$

Here $r_{ab}$ denotes the Fresnel reflection coefficients, where an incident wave with $b$ polarization is accompanied by a reflected wave with $a$ polarization ($a$ and $b$ stand for either the $s$ or $p$

component), and $r_{ab}(\theta_i)$ corresponds to the central wave vector at the incident angle $\theta_i$.

Putting everything together, we can obtain the reflected angular spectrum of the practical polarized Gaussian beam in the case of horizontal polarization:

$$\widetilde{\mathbf{E}}_r = \frac{r_{pp}(\theta_i)}{\sqrt{2}}\left\{\exp[k_{rx}(+i\eta-\vartheta)]\exp(+ik_{ry}\delta)\right. \\ \left.-i\frac{r_{sp}(\theta_i)}{r_{pp}(\theta_i)}\right\}\widetilde{\mathbf{E}}_{r+}+\frac{r_{pp}(\theta_i)}{\sqrt{2}}\left\{\exp[k_{rx}(-i\eta-\vartheta)]\right. \\ \left.\times\exp(-ik_{ry}\delta)+i\frac{r_{sp}(\theta_i)}{r_{pp}(\theta_i)}\right\}\widetilde{\mathbf{E}}_{r-}, \tag{6}$$

provided that $k_{rx}\eta \ll 1$, $k_{rx}\vartheta \ll 1$, and $k_{ry}\delta \ll 1$. In the above equation $\eta = (\partial r_{sp}/\partial\theta_i)/r_{pp}(\theta_i)k_0$, $\vartheta = (\partial r_{pp}/\partial\theta_i)/r_{pp}(\theta_i)k_0$, and $\delta = [1 + r_{ss}(\theta_i)/r_{pp}(\theta_i)]\cot\theta_i/k_0$. The terms $\exp(\pm ik_{rx}\eta)$ and $\exp(\pm ik_{ry}\delta)$ represent the spin-orbit coupling. Here we can see that the spin-orbit coupling related items $\eta$ and $\delta$ are affected by the axion coupling effect. It is well known that the photonic SHE manifests itself as the spin-orbit coupling, and so the in-plane and transverse spin-dependent splitting can be modulated through the axion coupling effect. Additionally, the other electric-field components $\exp(-ik_{rx}\vartheta)$ and $ir_{sp}(\theta_i)/r_{pp}(\theta_i)$ are not the spin-orbit coupling terms; however, they can affect the spin-dependent splitting. Especially, the term $ir_{sp}(\theta_i)/r_{pp}(\theta_i)$ also plays a great role in Kerr rotation. We note that the correction proportional to wave-vector component $k_{ix}$, ignored by previous work, is responsible for the in-plane spin-dependent splitting [25].

The photonic SHE is described for the left- and right-circularly polarized components undergoing the in-plane and transverse shifts, and so the reflected field centroid should be determined. At any given plane $z_a = \text{const}$, the displacements of the field centroid compared to the geometrical-optics prediction is given by

$$\delta_{\pm}^{x,y} = \frac{\iint \tilde{\mathbf{E}}^* i\partial_{\mathbf{k}_\perp}\tilde{\mathbf{E}}dk_{rx}dk_{ry}}{\iint \tilde{\mathbf{E}}^*\tilde{\mathbf{E}}dk_{rx}dk_{ry}}. \tag{7}$$

Here $\delta_{\pm}^{x,y} = \delta_{\pm}^{x}\mathbf{e}_{rx} + \delta_{\pm}^{y}\mathbf{e}_{ry}$ and $\partial_{\mathbf{k}_\perp} = \frac{\partial}{\partial k_{rx}}\mathbf{e}_{rx} + \frac{\partial}{\partial k_{ry}}\mathbf{e}_{ry}$. Substituting Eq. (6) into Eq. (7), we can get the in-plane and transverse spin-dependent displacements. It should be noted that, according to Eq. (6), we only consider the electric-field component $\exp[k_{rx}(\pm i\eta-\vartheta)]\exp(\pm ik_{ry}\delta)$ including the spin-orbit coupling part for field centroid calculation. Hence the in-plane and transverse spin-dependent shifts in the photonic SHE can be obtained.

## III. RESULTS AND DISCUSSION

When a linearly polarized light reflects from a medium surrounded by the magnetic field, the polarization plane undergoes a rotation due to the magneto-optical Kerr effect [30,31]. The Kerr effect can be used for determining the surface sensitivity of a material, studying a magnetic material on account of its robustness, and so on [32]. Here we investigate the Kerr rotation angles changing with different axion coupling under the condition of an external magnetic field. We only consider the incident light beam with horizontal polarization.

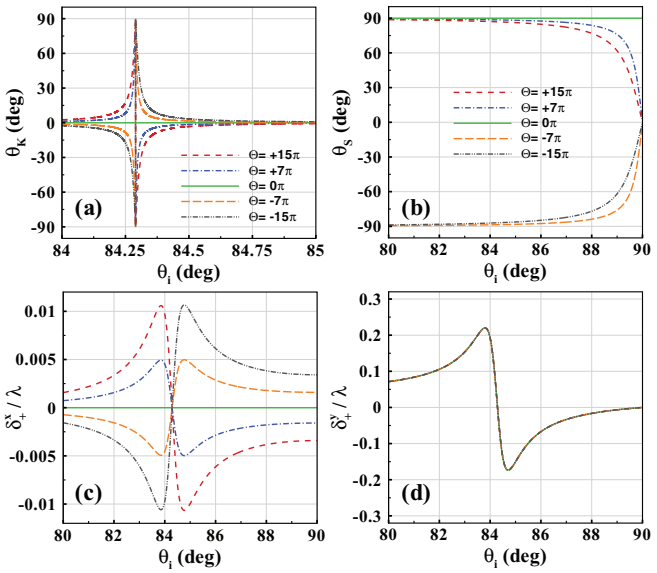


FIG. 2. (Color online) The photonic SHE and magneto-optical Kerr effect induced by axion coupling at air-TI interfaces in the case of horizontal polarization. Here the parameters are the refractive index of TIs $n = 10$ (appropriate for the TIs such as $Bi_{1-x}Se_x$). The beam waist is selected as $w_0 = 20\lambda$. (a) Kerr rotation angle with different axion angles. (b) Spin-dependent splitting rotation angle which satisfies the relationship $\tan\theta_S = \delta_+^y/\delta_+^x$. (c) and (d) In-plane and transverse displacements, respectively.

The direction of Kerr rotation is referred to the polarization direction of reflected light's central wave vector. Generally speaking, under the condition of horizontal polarization, the polarization direction of reflected light's central wave vector acquires no rotation for the absence of axion coupling, and so there is no Kerr effect. When time-reversal breaking perturbation is introduced on the TI surface, the material becomes fully gapped and the axion coupling effect happens, which induces the Kerr effect.

The axion angle $\Theta$ is shown to be quantized in odd integer values of $\pi$: $\Theta = (2n+1)\pi$, where $n \in \mathbb{Z}$. Here we choose the axion angle as $\Theta = 0, \pm 7\pi, \pm 15\pi$, and the refractive index of the TIs is chosen as $n = 10$ (appropriate for the TIs such as $Bi_{1-x}Se_x$) [8]. The beam waist is selected as $w_0 = 20\lambda$. Figure 2(a) shows the Kerr rotation angle $\theta_K$ versus the incident angle $\theta_i$ for horizontal polarization. Since $\theta_K$ represents tiny values for $\theta_i$ in the range of 0 to 84° and 85 to 90°, the attention is focused on the range of 84 to 85°. The Kerr rotation can be enhanced with the increasing of axion angle $\Theta$. Surprisingly, we can see that the magnitude of the Kerr angle can reach about 90° at a fixed incident angle about 84.3°. In addition, the Kerr angle $\theta_K$ reverses its direction when the axion angle changes sign, so that we can easily manipulate the Kerr rotation by adjusting the axion angle.

In fact, the Kerr rotation in TIs is accompanied by the photonic SHE, which was not considered previously. Next we numerically discuss this effect and reveal the unusual results caused by the axion coupling. The spin-dependent splitting rotation angle manifesting for the relationship $\tan\theta_S = \delta_+^y/\delta_+^x$ is illustrated in Fig. 2(b). It represents some interesting properties with different axion angles. The results

can be explained by considering the in-plane and transverse spin-dependent splitting, respectively. First, we analyze the in-plane one. In past work, the in-plane spin-dependent splitting cannot be observed in the case of horizontal polarization or vertical polarization [25]. However, in present research, this effect surprisingly happens in these two polarized states. The reason is ascribed to the axion coupling effect induced nonzero cross-polarized reflection coefficients $r_{ps}$ and $r_{sp}$ from Eq. (2). However, at the usual air-glass interface, the cross-polarized reflection coefficients are equal to zero, and so the in-plane spin-dependent splitting cannot be observed. Remarkably, as we will investigate in the following, the in-plane shifts are very sensitive to the value of the axion angle, and so the tunable value and sign of the axion angle allow us to describe a method for modulating the in-plane spin-dependent splitting.

Figure 2(c) shows the in-plane shifts in the photonic SHE changing with the incident angle and the axion angle. Here we just consider the left-circularly polarized component, and the polarized state is chosen as horizontal polarization. For a positive (or negative) axion angle ($\Theta \neq 0$), the absolute values of the in-plane shifts first rise with the increasing of incident angle. Then the displacements decrease after moving away from the maximum and reach the negative maximum value. For a fixed incident angle, the absolute values of the displacements increase when the axion angle grows ($\Theta = \pm 7\pi, \pm 15\pi$). When the axion angle changes its sign, the in-plane shifts reverse their direction too. Obviously, the in-plane spin-dependent splitting is sensitive to the variations of the axion angle. Therefore we can determine the values of the axion coupling by detecting the in-plane shifts of the photonic SHE or modulate the in-plane displacements by manipulating the magnitude of the axion angle. It should be noted that, as for the TIs, the in-plane spin-dependent splitting originates from the axion coupling effect. If we set the axion angle $\Theta = 0$, the Fresnel coefficients obtained from Eq. (1) can reduce to the result of usual media such as BK-7 glass and the in-plane spin-dependent splitting disappears.

The transverse spin-dependent splitting in the photonic SHE is described in Fig. 2(d). We also calculate the transverse shifts varying with the incident angle $\theta_i$ and axion angle $\Theta$. For a given axion angle, the transverse displacements first rise with the increase of $\theta_i$. After reaching the peak value at the incident angle of about 83.6°, the shift decreases rapidly and then reaches the negative maximum value. As shown, the transverse displacements can be tuned to a negative or positive value by adjusting the incident angle, which represents a switchable property. However, with the variations of axion angle $\Theta$, the transverse shifts are almost identical. That is to say, the transverse spin-dependent splitting is insensitive to the axion coupling effect. In fact, there really exist tiny differences between various displacement curves, but these differences are too small to be distinguished in the picture. It should be noted that, however, the transverse displacements can represent a significant variation when the axion angle is chosen as a large value.

From Eq. (6), the electric-field component $\exp[k_{rx}(\pm i\eta - \vartheta)]\exp(\pm ik_{ry}\delta)$ including the spin-orbit coupling part is used for field centroid calculation. However, it also affects the polarization structure of the Kerr effect for certain incident angle ranges, and the other electric-field component $ir_{sp}(\theta_i)/r_{pp}(\theta_i)$ takes a great role in Kerr rotation. Figures 3(a)–3(d) show the electric-field intensity and polarization distribution of these two components. Here the incident angle is chosen as 83 or 89° and the axion angle is selected as $+7\pi$. From Figs. 3(a) and 3(c), we can see that the polarization is mainly in the vertical direction. When the incident angle is less than about 84°, the electric-field component $ir_{sp}(\theta_i)/r_{pp}(\theta_i)$ represents a tiny value and the first spin-orbit coupling electric-field component can affect the Kerr rotation. Therefore the Kerr angle shows a small rotation. As the incident angle increases, the second component plays a major role in the Kerr rotation and the Kerr angle can reach a huge value (about 90°). Figures 3(b) and 3(d) describe the electric-field intensity of the spin-orbit coupling component. Here the blue arrows, circles, and ellipses represent the polarization distribution. When the spin-dependent splitting occurs, the photons with opposite helicities accumulate at the opposite edges of the beam.

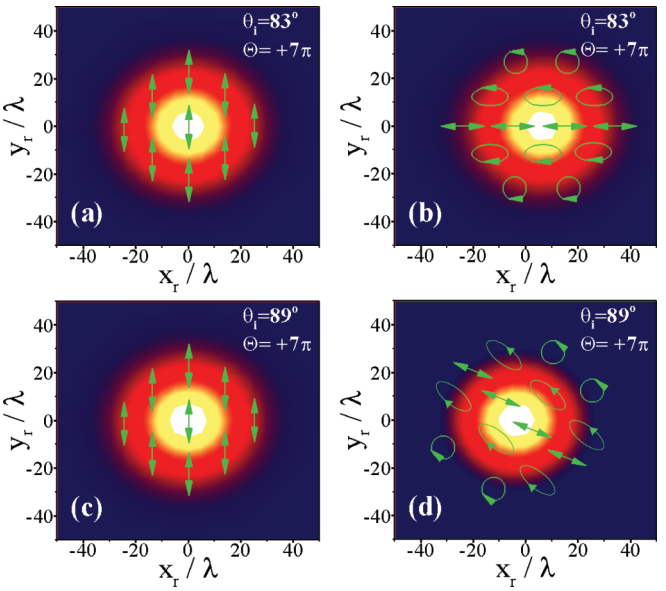


FIG. 3. (Color online) Schematic diagram for electric-field intensity and polarization distribution of the light beam. Here the parameters are $\theta_i = 83$ and 89° and $\Theta = +7\pi$. (a) and (c) Intensity and polarization distribution without considering the spin-orbit coupling electric-field component. (b) and (d) Spin-orbit coupling conditions. The intensity is plotted in normalized units.

Generally speaking, the photonic SHE including in-plane and transverse spin-dependent splitting can be explained by the cross-polarized effect [12]. The superposition of the main electric-field and cross-polarized electric-field components finally causes the photons with opposite helicities to accumulate at the opposite edges of the beam, which is a feature of spin-dependent splitting. In this work, owing to the axion coupling effect, the polarization direction of reflected light's central wave vector changes by a tiny value, showing a difference with the initial polarization direction. Thus, the direction of the cross-polarized electric-field vector is also not perpendicular to the initial polarization direction. It is perpendicular to the polarization direction of reflected light's central wave vector.

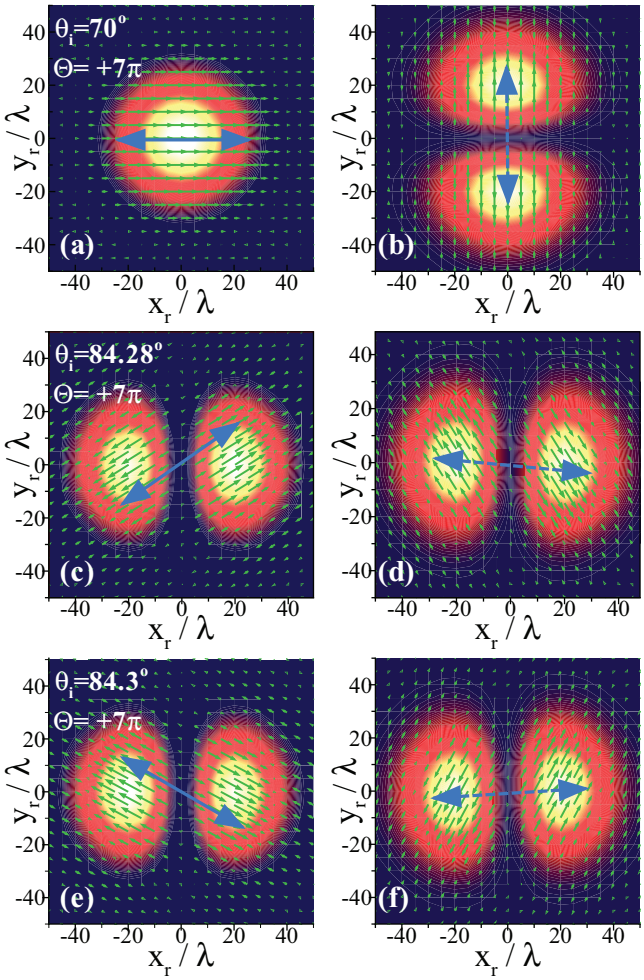


FIG. 4. (Color online) The main electric-field and cross-polarized electric-field components of the light beam reflected on the TI interface. Here, the tiny arrows denote the direction of the electric-field vector, and the axion angle is chosen as $\Theta = +7\pi$. (a), (c), and (e) Main electric-field distribution for different incident angles. The solid arrows represent the direction of the Kerr rotation. (b), (d), and (f) Cross-polarized electric-field components. Here the dashed arrows stand for the direction of spin-dependent splitting and the intensity is plotted in normalized units.

We note that the analysis of the cross-polarized effect is useful for studying both the Kerr rotation and photonic SHE.

According to Eq. (4), we can obtain the reflected electric field by employing the Fourier transformations. Figure 4 describes the cross-polarized effect of the light beam reflected on the TI interface. Here the calculation parameters are chosen the same as in Fig. 2. Figures 4(a), 4(c), and 4(e) show the main electric-field distribution of the reflected beam. We draw not only the electric-field intensity but also the electric-field vector. In the above analysis, we know that the direction of Kerr rotation can be registered in the polarization direction of reflected light's central wave vector. From the picture, we can see that the direction of the central electric-field vector (the small arrows) undergoes a rotation with different incident angles, and so the Kerr effect also rotates its direction (the solid arrows). The cross-polarized components are described in Figs. 4(b), 4(d), and 4(f). It is noted that the cross-polarized effect stands for photons with opposite helicities accumulated at the opposite edges of the beam. Therefore the direction of the cross-polarized electric-field intensity distribution can be regarded as the direction of spin-dependent splitting (the dashed arrows). We can select the cross-polarized components by adding a polarizer with the optical axis perpendicular to the polarization direction of reflected light's central wave vector. In this condition the shape of the cross-polarized electric-field intensity represents a symmetrical double-peak distribution, which can be seen as a reference. We rotate the polarizer until we get this symmetrical double-peak distribution. Then the Kerr angle can be obtained from the rotation angle of the polarizer.

The axion coupling effect is an important phenomenon, yet it is hard to observe experimentally. Some theoretical methods have been proposed to detect this effect, such as measuring the Faraday rotation angle and the Goos-Hänchen displacements [7,8]. Here we also theoretically propose an optical method, the signal enhancement technique known as weak measurement [33,34], to measure this topological phenomenon. Note that the weak measurement technique has attracted a lot of attention and holds great promise for precision metrology [35–38]. In previous works, the in-plane and transverse spin-dependent splittings were measured by using this technique [25,29,39]. We have established the relationship between the axion angle and photonic SHE induced displacements. If these displacements can be measured, we can determine the strength of axion coupling. However, under this condition, the transverse shifts are insensitive to the variations of the axion angle. Therefore we choose to measure the axion coupling by detecting the in-plane shifts with weak measurements.

Figure 5 denotes the weak measurement theory and results for measuring the in-plane spin-dependent splitting. The detailed equipment description and experiment analysis can be found in previous works [28,29,39]. All of the above experimental equipment is suitable for the particular wavelength (for the refractive index $n = 10$ of TIs). In fact, there exist two types of amplified factors $A_w$ and $F$ similar to those in Ref. [13], which gives an enhanced displacement proportional to the initial one, $\delta_w = A_w^{\mathrm{mod}}\delta_+^x$. Here $A_w^{\mathrm{mod}} = |A_w|F$, and $\delta_+^x$ and $\delta_w$ represent the initial and amplified in-plane shifts. Figure 5(a) shows that the preselection and postselection polarization give rise to an interference in the observation plane, shifting it to its final centroid position proportional to $A_w = \delta_w/\delta_+^x$. It is noted that the imaginary $A_w$ denotes a shift in momentum space corresponding to free evolution of the beam. Then the amplified factor turns out to be $A_w^{\mathrm{mod}} = |A_w|F$, which can be much larger than $A_w$. The extra amplified factor $F$ depends on the initial state of the beam and the degree of its free evolution before the observer [Fig. 5(b)].

The incident beam is focused by the lens and is preselected in the horizontal polarization, and then it is postselected in the polarization state with $\mathbf{V} = \cos\varphi\mathbf{e}_{rx} + \sin\varphi\mathbf{e}_{ry}$. Here $\varphi = \arctan(r_{sp}/r_{pp}) + \pi/2 + \Delta$. We note that, in the previous weak measurement system [29], the two polarizations are nearly perpendicular to each other with an angle of $90^\circ \pm \Delta$. The relevant amplitude of the reflected field at a plane can be obtained as $\mathbf{V}\cdot\mathbf{E}_r$, allowing for calculation of amplified displacement. Here the free evolution of the light beam between the position of the initial focused waist and the

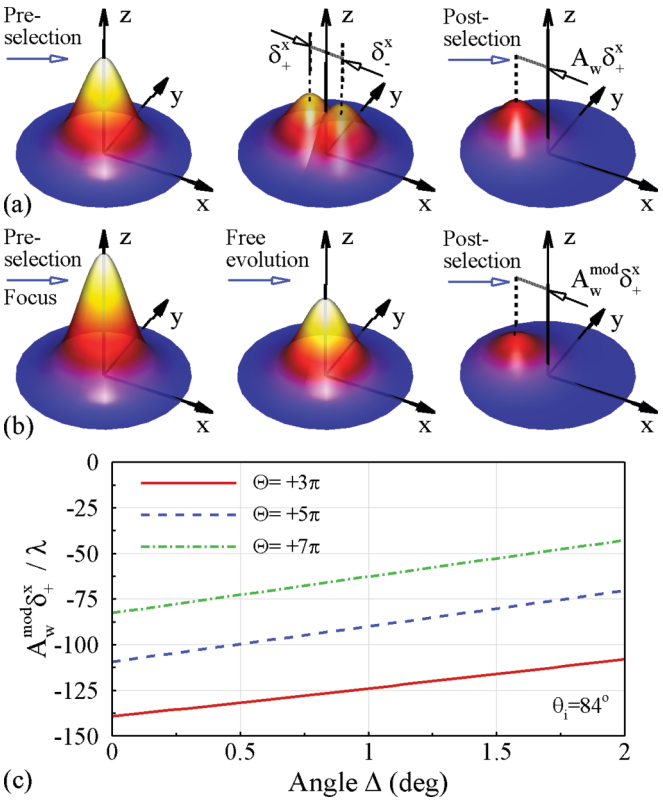


FIG. 5. (Color online) The theory and results of weak measurements for measuring the axion coupling effect. (a) The two circularly polarized components interfering destructively after the second polarizer so that the spin-dependent shifts are significantly amplified with the amplified factor $A_w$. (b) The case in which both the pre- and postselection mechanisms and the free propagation of the light beam are involved, and so the final centroid is proportional to $A_w^{\mathrm{mod}}$, which can be much lager than $A_w$. (c) Amplified in-plane displacements changing with the variation of axion angle $\Theta$ and amplified angle $\Delta$. The incident angle is fixed to $\theta_i = 84^\circ$ and the observation plane is selected as $z_r = 200 z_R$. Here $z_R = k_0 w_0^2/2$, $w_0$ is the beam waist.

position of the observer plays a great role in the amplified factor $F$. The theoretical amplified shifts are shown in Fig. 5(c). Here the incident angle is fixed to 84°. Then we obtain the amplified displacements varying with axion angle and amplified angle $\Delta$. For a fixed angle $\Delta$, the amplified in-plane shifts change clearly with the different axion angles ($\Theta = +3\pi, +5\pi$, and $+7\pi$), and so we can measure the axion coupling effect by determining the in-plane displacements with weak measurements.

## IV. CONCLUSIONS

In conclusion, we have examined the photonic spin Hall effect (SHE) of a light beam reflected from the air-topological insulator (TI) interface due to axion coupling. We have found that the spin-orbit coupling in the photonic SHE can be routed by adjusting the strength of the axion coupling. The in-plane spin-dependent splitting is sensitive to the axion angle variations of TIs, and so the enhanced and switchable in-plane shifts were observed with different axion coupling. However, the transverse spin-dependent splitting is insensitive to the axion coupling in the case of an axion angle with a small value. We have also found that, by adjusting the axion angle, the magnitude and direction of the Kerr rotation angle can be modulated. In addition, the field structure for the reflected beam has been analyzed. The cross-polarized effect induced symmetrical double-peak field structure can be used to determine the Kerr rotation. Importantly, a signal enhancement technique known as weak measurement has been theoretically proposed to measure this topological phenomenon. These findings offer us potential methods for determining the strength of the axion coupling and provide new insight into the interaction of light with TIs.

## ACKNOWLEDGMENT

This research was partially supported by the National Natural Science Foundation of China (Grants No. 61025024 and No. 11274106).

[1] J. E. Hirsch, Phys. Rev. Lett. **83**, 1834 (1999).
[2] Y. K. Kato, R. C. Myers, A. C. Gossard, and D. D. Awschalom, Science **306**, 1910 (2004).
[3] V. Sih, Y. K. Kato, and D. D. Awschalom, Phys. World **18**, 33 (2005).
[4] X. L. Qi and S. C. Zhang, Phys. Today **63**, 33 (2010).
[5] J. E. Moore, Nat. Phys. **5**, 378 (2009).
[6] L. Fu, C. L. Kane, and E. J. Mele, Phys. Rev. Lett. **98**, 106803 (2007).
[7] J. Maciejko, X. L. Qi, H. D. Drew, and S. C. Zhang, Phys. Rev. Lett. **105**, 166803 (2010).
[8] M. C. Chang and M. F. Yang, Phys. Rev. B **80**, 113304 (2009).
[9] A. Bernevig, T. Hughes, and S. C. Zhang, Science **314**, 1757 (2006).
[10] X. L. Qi and S. C. Zhang, Rev. Mod. Phys. **83**, 1057 (2011).
[11] M. Onoda, S. Murakami, and N. Nagaosa, Phys. Rev. Lett. **93**, 083901 (2004).
[12] K. Y. Bliokh and Y. P. Bliokh, Phys. Rev. Lett. **96**, 073903 (2006).
[13] O. Hosten and P. Kwiat, Science **319**, 787 (2008).
[14] K. Y. Bliokh, A. Niv, V. Kleiner, and E. Hasman, Nat. Photon. **2**, 748 (2008).
[15] A. Aiello and J. P. Woerdman, Opt. Lett. **33**, 1437 (2008).
[16] H. Luo, S. Wen, W. Shu, Z. Tang, Y. Zou, and D. Fan, Phys. Rev. A **80**, 043810 (2009).
[17] N. Hermosa, A. M. Nugrowati, A. Aiello, and J. P. Woerdman, Opt. Lett. **36**, 3200 (2011).
[18] P. Gosselin, A. Bérard, and H. Mohrbach, Phys. Rev. D **75**, 084035 (2007).
[19] C. A. Dartora, G. G. Cabrera, K. Z. Nobrega, V. F. Montagner, M. H. K. Matielli, F. K. R. de Campos, and H. T. S. Filho, Phys. Rev. A **83**, 012110 (2011).
[20] J.-M. Ménard, A. E. Mattacchione, M. Betz, and H. M. van Driel, Opt. Lett. **34**, 2312 (2009).

[21] J.-M. Ménard, A. E. Mattacchione, H. M. van Driel, C. Hautmann, and M. Betz, Phys. Rev. B **82**, 045303 (2010).
[22] N. Shitrit, I. Bretner, Y. Gorodetski, V. Kleiner, and E. Hasman, Nano Lett. **11**, 2038 (2011).
[23] Y. Gorodetski, K. Y. Bliokh, B. Stein, C. Genet, N. Shitrit, V. Kleiner, E. Hasman, and T. W. Ebbesen, Phys. Rev. Lett. **109**, 013901 (2012).
[24] N. Shitrit, I. Yulevich, E. Maguid, D. Ozeri, D. Veksler, V. Kleiner, and E. Hasman, Science **340**, 724 (2013).
[25] Y. Qin, Y. Li, X. Feng, Y.-F. Xiao, H. Yang, and Q. Gong, Opt. Express **19**, 9636 (2011).
[26] H. Wang and X. Zhang, Phys. Rev. A **83**, 053820 (2011).
[27] G. Xu, T. Zang, H. Mao, and T. Pan, Phys. Rev. A **83**, 053828 (2011).
[28] X. Zhou, Z. Xiao, H. Luo, and S. Wen, Phys. Rev. A **85**, 043809 (2012).
[29] H. Luo, X. Zhou, W. Shu, S. Wen, and D. Fan, Phys. Rev. A **84**, 043806 (2011).
[30] T. Katayama, Y. Suzuki, H. Awano, Y. Nishihara, and N. Koshizuka, Phys. Rev. Lett. **60**, 1426 (1988).
[31] W. K. Tse and A. H. MacDonald, Phys. Rev. Lett. **105**, 057401 (2010).
[32] M. Buchmeier, R. Schreiber, D. E. Burgler, and C. M. Schneider, Phys. Rev. B **79**, 064402 (2009).
[33] Y. Aharonov, D. Z. Albert, and L. Vaidman, Phys. Rev. Lett. **60**, 1351 (1988).
[34] N. W. M. Ritchie, J. G. Story, and R. G. Hulet, Phys. Rev. Lett. **66**, 1107 (1991).
[35] G. J. Pryde, J. L. O'Brien, A. G. White, T. C. Ralph, and H. M. Wiseman, Phys. Rev. Lett. **94**, 220405 (2005).
[36] P. B. Dixon, D. J. Starling, A. N. Jordan, and J. C. Howell, Phys. Rev. Lett. **102**, 173601 (2009).
[37] J. Dressel and A. N. Jordan, Phys. Rev. Lett. **109**, 230402 (2012).
[38] M. R. Dennis and J. B. Götte, New J. Phys. **14**, 073013 (2012).
[39] X. Zhou, X. Ling, H. Luo, and S. Wen, Appl. Phys. Lett. **101**, 251602 (2012).